2-3

Numerical Analysis of Thermochemical Nonequilibrium Hypersonic Flow around Blunt Body

Takuji KUROTAKI
Kamakura Works, Mitsubishi Electric Corporation, Kamakura, Japan

Abstract

Numerical analyses of chemically and thermally nonequilibrium hypersonic flow around a blunt body are carried out. Several types of flow; Problem I (Sphere cases), Problem II. 1-3 (Orex cases) and Problem IV. 1-2 (Spherically Blunted Cone cases) specified in the "High Enthalpy Flow Workshop" are investigated.

Axisymmetric full Navier-Stokes equations which have chemically and thermally nonequilibrium effects are considered by using Park's two-temperature model and the vibrational relaxation model from the SSH theory. For the time integration, an efficient numerical algorithm of an implicit finite difference method is used, which consists of the combination of LU-SGS scheme and the implicit diagonal method for a source Jacobian matrix. For convective terms, AUSMDV scheme generalized into the nonequilibrium flow case is applied.

Some numerical results of each flow cases are presented and discussed. All cases indicate that the flow inside the shock layer is in strong nonequilibrium and very complex real gas effects are observed. It is shown that fairly reasonable results can be obtained with both numerical methods and physical models applied here. However, numerical results of some cases indicate that more careful analyses and comparison with experimental results are necessary in order to clarify the more complex flow structures in the back flow region.

1. Introduction

When designing reentry vehicles such as capsules or space shuttle-type space planes, it is important to predict the very severe aerodynamic heating around the body at an high altitude. However, it is almost impossible now to get all the solutions from only wind tunnel experiments since their flight is at high Mach number and the temperature inside the shock layer usually becomes very high. Therefore, numerical analysis is a hopeful approach and it is now becoming a main tool to get information of the flow at real flight conditions.

Because the flow contains the strong shock wave, the numerical scheme should be the one with high resolution and robustness for discontinuities. Furthermore, the presence of real gas effects such as dissociation or ionization etc. in these flight regime complicates the flow characteristics drastically and even the influence of chemical and thermal nonequilibrium should be sometimes considered. Therefore, careful validation of both the numerical scheme and the physical models are necessary.

In this paper, the numerical methods and physical models applied in the analyses of the problem specified in the "High Enthalpy Flow Workshop" are mentioned and several numerical examples of the results are presented and discussed. The flow cases analyzed in this study are Problem I (Sphere cases), Problem II. 1-3 (Orex cases) and Problem IV. 1-2 (Spherically Blunted Cone cases).

2. Governing Equations and Numerical Methods

We consider axisymmetric full Navier-Stokes equations as governing equations. Air is assumed to have 7 species (O_2, N_2, O, N, NO, NO^+, e^-) and steady and laminar flow is considered for all cases.

In order to include thermal-chemical nonequilibrium effects in numerical analyses, Park's two-temperature model is used [1]. In this model, an assumption that the translational and rotational energy modes are in equilibrium at the translational temperature T, while the vibrational, electronic and electron-translational modes are in equilibrium at the vibrational temperature Tv, is employed.

The governing equations under these assumptions in the Cartesian coordinate system are

$$\frac{\partial Q}{\partial t} + \frac{\partial}{\partial x}(E - E_v) + \frac{\partial}{\partial y}(F - F_v) + \alpha H = S + \alpha H_v , \quad (1)$$

where

$$\alpha = \begin{cases} 0 & \text{for a two-dimensional flow} \\ 1 & \text{for an axisymmetric flow} \end{cases} , \quad (2)$$

$$Q = \begin{bmatrix} \rho u \\ \rho v \\ E_t \\ E_{vib}+E_e \\ \rho_s \end{bmatrix}, E = \begin{bmatrix} \rho u^2 + p \\ \rho uv \\ u(E_t + p) \\ u(E_{vib}+E_e) \\ \rho_s u \end{bmatrix}, F = \begin{bmatrix} \rho uv \\ \rho v^2 + p \\ v(E_t + p) \\ v(E_{vib}+E_e) \\ \rho_s v \end{bmatrix} \quad (3)$$

and the vector E_v and F_v are a set of elements of viscous

terms in the ξ and η-direction respectively. The vector S is a set of elements of source terms. H and H_v are a set of elements of convective and viscous terms respectively added only when the flow is axisymmetric. In eq. (3), the quantities ρ, p, E_t, E_{vib} and E_e denote density, pressure, the total energy per unit volume, the vibrational energy per unit volume and the electronic energy per unit volume respectively. The quantities u and v are velocity components. The subscript "s" denotes a species of air.

For chemical reaction rates, the model proposed by Park is used, and the forward reaction rate is assumed to be the function of $\sqrt{T\,T_v}$ and the following twenty-four chemical reactions are assumed,

(1) $O_2+M \rightleftarrows O+O+M$, M = O_2, N_2, O, N, NO, NO^+, e^-

(2) $N_2+M \rightleftarrows N+N+M$, M = O_2, N_2, O, N, NO, NO^+, e^-

(3) $NO+M \rightleftarrows N+O+M$, M = O_2, N_2, O, N, NO, NO^+, e^-

(4) $O+NO \rightleftarrows N+O_2$

(5) $O+N_2 \rightleftarrows N+NO$

(6) $O+N \rightleftarrows NO^+ + e^-$.

Transport properties such as viscosity, thermal conductivity and diffusion coefficients are calculated from the kinetic theory described in [1], [2].

The governing equations (1) is solved by a finite difference method after non-dimensionalized and transformed into the general coordinate system. In this study, the implicit formulation is used and Lower-upper symmetric Gauss-Seidel (LU-SGS) scheme [3] is applied for the time integration of the system. In this scheme, no matrices need not be inverted and, especially for the use of a parallel computer, very high efficiency can be achieved since it can be completely vectorizable. Some difficulties arise, however, when LU-SGS scheme is directly applied to the flow with finite-rate chemistry because coefficient matrices include a Jacobian matrix of source vector S which is dense. In order to avoid these difficulties, the diagonal implicit method [4] is applied in which the Jacobian matrix of S is approximated to a diagonal matrix whose elements are the function of characteristic time for chemical reactions [4, 5].

Since the hypersonic flow, in general, contains very strong shock wave systems, the numerical scheme with high resolution and robustness should be used for the evaluation of convective terms . Most of such high resolution schemes are categorized as Flux Difference Splitting (FDS) or Finite Vector Splitting (FVS). Roe scheme is one of the most popular one among FDS schemes, however it has a serious problem, so-called "carbuncle phenomenon", in capturing a strong shock around a stagnation region. FVS schemes are more robust in multi-dimensional calculations but they are too dissipative in shear layers such as boundary layers to apply for Navier-Stokes flow analyses.

Recently, some new approaches to develop less dissipative upwind schemes are reported, in which the large dissipation of FVS is reduced by introducing the flavor of FDS into FVS schemes. One of examples of them is Advection Upstream Splitting Method (AUSM) and some variations of it are reported [6].

In this study, AUSMDV proposed by Wada and Liou [6] is applied after being generalized into nonequilibrium flow cases. This scheme is mixture of AUSMD-type (flux-difference-splitting-biased) schemes and AUSMV-type (flux-vector-splitting-biased) ones and is recognized as an improved AUSM scheme because numerical overshoot immediately behind the shock is removed. In order to remove the carbuncle phenomenon in calculating the flow which contains a very strong shock in front of the stagnation region, their approach is also applied, in which Hänel's FVS scheme is used only immediately after the shock wave.

3. Physical Models for Vibrational Relaxation Time

In order to include thermal nonequilibrium effects in the numerical analyses, the following vibrational relaxation term which appears in the vibrational-electronic energy equation plays an important role,

$$\frac{\overline{E_{vib,s}} - E_{vib,s}}{\tau_{s,q}} \qquad (4)$$

where $E_{vib,s}$ is the vibrational energy of molecule s per unit volume, $\tau_{s,q}$ is a vibrational relaxation time of molecule s colliding with a chemical species q and " $\bar{}$ " denotes that the quantity is in thermal equilibrium.

Usually a semi empirical law proposed by Millikan and White based on the the Landau-Teller theory is used in order to calculate $\tau_{s,q}$,

$$p\tau_{s,q} = \exp\left[1.16\times10^{-3}\mu_{s,q}^{1/2}\theta_{v,s}^{4/3}\left(T^{-1/3} - 0.015\mu_{s,q}^{1/4}\right) - 18.42\right] \qquad (5)$$

where p is pressure in atmospheres, $m_{s,q}$ is reduced mass in grams and $\theta_{v,s}$ is vibrational characteristic temperature of molecule s. However, it is well known that this model underestimates $\tau_{s,q}$ when translational temperature is more than about 8,000 K since this model neglects the collision frequency and $\tau_{s,q}$ loses even physical meaning at a certain temperature as it becomes smaller than the collision time.

In this study, the another model from the SSH theory proposed by Schwartz, Slawsky and Herzfeld [7, 8] in 1950's is applied to evaluate $\tau_{s,q}$. Under the assumptions that the molecule is a harmonic oscillator and only monoquantum transition of vibrational energy modes is allowed, $\tau_{s,q}$ is expressed as,

$$1/\tau_{s,q} = Z_{col}^{sq} P_{10}(A_s, A_q)\left[1 - \exp\left(-\theta_{v,s}/T\right)\right] \qquad (6)$$

where Z^{sq}_{coll} is collision frequency of molecule s with a chemical species q, $P_{10}(A_s, A_q)$ is transition probability in which vibrational energy level changes from 1 to 0. Furthermore, transition probability $P_{10}(A_s, A_q)$ in the SSH theory has the following form,

$$P_{10}(A_s, A_q) = A / (Z^s_0 \; Z^s_v \; Z^{sq}_T \; Z^{sq}_+) \qquad (7)$$

where A is a collision cross-reference factor, Z^s_0 is a steric factor, Z^s_v is a vibrational factor, Z^{sq}_T is a translational factor and Z^{sq}_+ is a factor from the attractive force.

Figure 1 and 2 show τ_{O_2,O_2} for O_2-O_2 collision and τ_{N_2,N_2} for N_2-N_2 collision respectively from both the Landau-Teller type model and the model from the SSH theory. There is clearly a difference between these models at very high translational temperature more than about 10,000K. Although the model from the SSH theory can reasonably predict a vibrational relaxation time at high temperature for molecule-molecule collision, it is reported that there is often disagreement between the result from this model and experimental data for molecule-atom collision such as O_2-O or N_2-O collision [8]. For these cases, the following semi empirical equations are used under the assumption that the relaxation times have the same temperature dependency as that in eq. (6),

$$p\,\tau_{O_2,O} = T^{2/3} \exp(33.4\, T^{-1/3} - 24.98)$$

$$p\,\tau_{N_2,O} = T^{2/3} \exp(49.7\, T^{-1/3} - 22.55).$$

Figure 3 shows $\tau_{O_2,O}$ and $\tau_{N_2,N}$ for both the Landau-Teller type model and the model from the SSH theory. For other relaxation times, we made the following assumptions,

$$p\,\tau_{NO,NO} = T^{2/3} \exp(75.6\, T^{-1/3} - 27.63)$$

$$p\,\tau_{O_2,N} = p\,\tau_{O_2,O}\;,\; p\,\tau_{N_2,N} = p\,\tau_{N_2,O} \qquad (9)$$

$$p\,\tau_{NO,s} = p\,\tau_{NO,NO} \quad (s = O_2, N_2, O, N, NO^+).$$

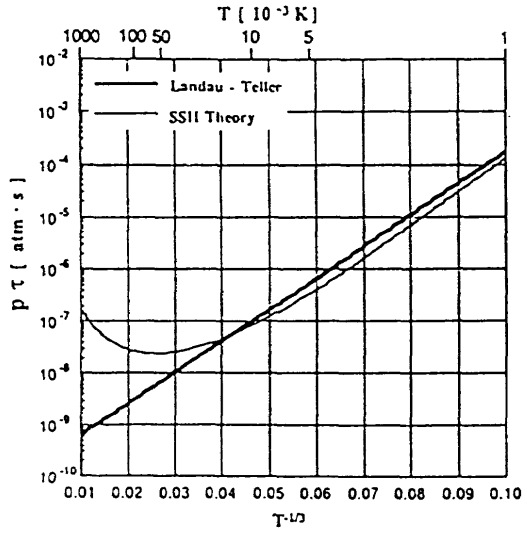

Fig.1 Relaxation time τ_{O_2,O_2} for O_2-O_2 collision

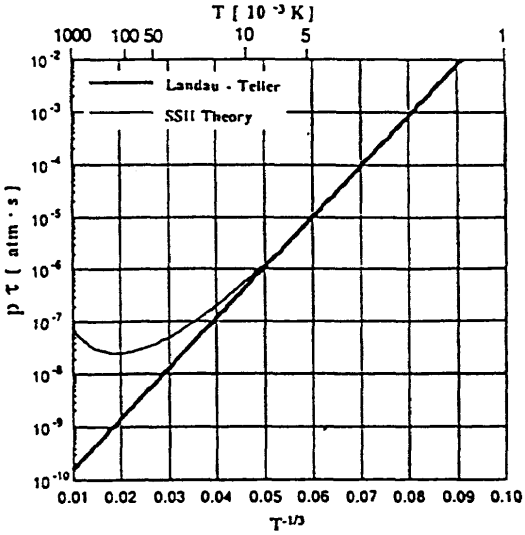

Fig.2 Relaxation time τ_{N_2,N_2} for N_2-N_2 collision

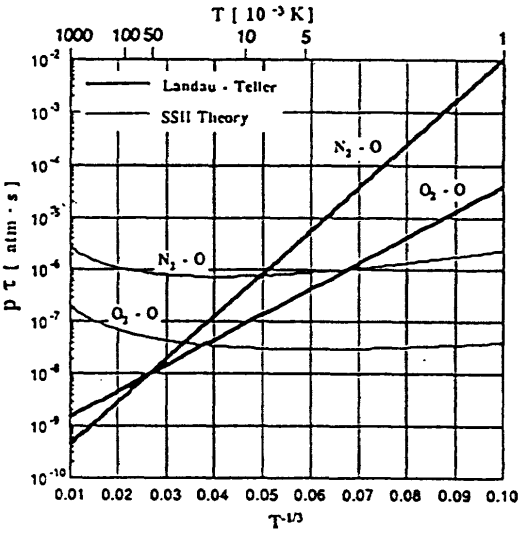

Fig.3 Relaxation time $\tau_{O_2,O}$ for O_2-O collision and $\tau_{N_2,N}$ for N_2-N collision

4. Wall Boundary Conditions

In this study, the gradient of pressure perpendicular to the wall is assumed to be zero, and for velocities and translational temperature, no slip boundary condition is applied along the wall. The wall vibrational temperature T_{v_w} is assumed to be the same as the translational temperature T_w at the wall which is specified in each flow cases.

The treatment of densities of each chemical species depends on whether the wall is catalytic or non-catalytic. When the wall is non-catalytic, the gradient of mass fraction of each species s perpendicular to the wall is assumed to be zero;

$$\frac{\partial c_s}{\partial \eta} = 0 \qquad (10)$$

where c_s is a mass fraction of a chemical species s, and η is coordinates perpendicular to the wall.

When the wall is catalytic, all O and N atoms colliding with the wall are assumed to become O_2 and N_2 molecules respectively through the recombination process at the wall, while for other species such as NO, NO^+, e^-, the wall is assumed to be non-catalytic and eq. (10) is applied. At so-called "p-plane" which is one mean-free path away from the wall, the mass flux of N atoms, for example, is expressed as using the Fick's law,

$$-k_N\rho_N = -\rho D_N\frac{\partial c_N}{\partial \eta}, \quad +k_N\rho_N = -\rho D_{N_2}\frac{\partial c_{N_2}}{\partial \eta} \qquad (11)$$

where k_s is catalytic velocity ($= \gamma\sqrt{kT_w/(2\pi m_s)}$), γ is catalytic efficiency, k is Boltzmann constant, m_s is a mass of one particle of a species s and D is a diffusion coefficient. By discretizing eq. (11) and under the assumption that $\rho_N = 0$ at the wall, we can get the expression of density of N_2 molecules at the wall in the following form,

$$\rho_{N_2,w} = \left(\rho_{N_2,j=2} + \frac{D_N}{D_{N_2}}\rho_{N,j=2}\right)\frac{\rho_w}{\rho_{j=2}} \qquad (12)$$

where the subscript "j = 2" denotes that the property is at the grid point next to the wall.

5. Numerical Results and Discussions

Figure 4. (a) - (d) show grid systems used in this study. The number of grid points is 81 in ξ-direction (along the body) and 81 in η-direction (perpendicular to the body) for Problem I and II and 161×131 for Problem IV. An algebraic method is applied to generate all grid systems.

So-called "Cell Reynolds number" at the wall around the stagnation region for each cases are determined after preliminary analyses and the quantity 0.2 for Problem I and II.1, 2.0 for Problem II.2 and II.3 and 1.0 for Problem IV are used. These preliminary calculations show that we should be very careful to determine a grid interval in η-direction at the wall especially for the case in which the wall temperature is low since this interval has a great influence on the heat flux at the wall even for such a sophisticated scheme as AUSMDV applied in this study.

Figure 5. (a) - (c) show the temperature distribution for Problem I.1, I.3 and I.5 respectively. These translational temperature distribution shown on the upper side are almost the same, while the vibrational temperature distribution shown on the under side depends on the free stream density condition. For the case in which the free stream density is relatively high such as Problem I.5, the vibrational temperature distribution become to resemble the translational one since the flow in the shock layer approaches the thermal equilibrium.

The heat flux Q along the wall for all cases of Problem I are shown in Figure 6, 7 and 8. The maximum heat flux at the stagnation point of a catalytic wall case is about 1.5 times higher than that of a non-catalytic case.

Figure 9 and 10 show the examples of results for Problem II.1 whose free stream conditions are corresponding to a flight at a very high altitude. The pressure distribution in Figure 9 and the translational and the vibrational temperature distribution along the stagnation streamline in Figure 10 indicate that the shock wave is thick and the flow inside the shock layer is in strong nonequilibrium.

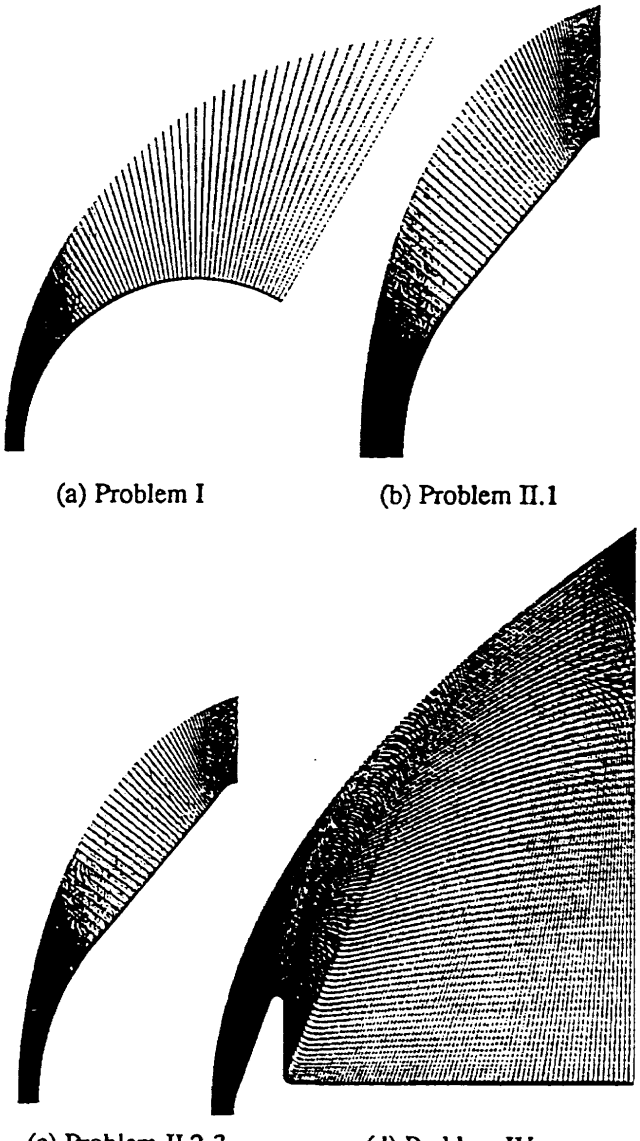

(a) Problem I (b) Problem II.1

(c) Problem II.2-3 (d) Problem IV

Fig.4 Mesh system

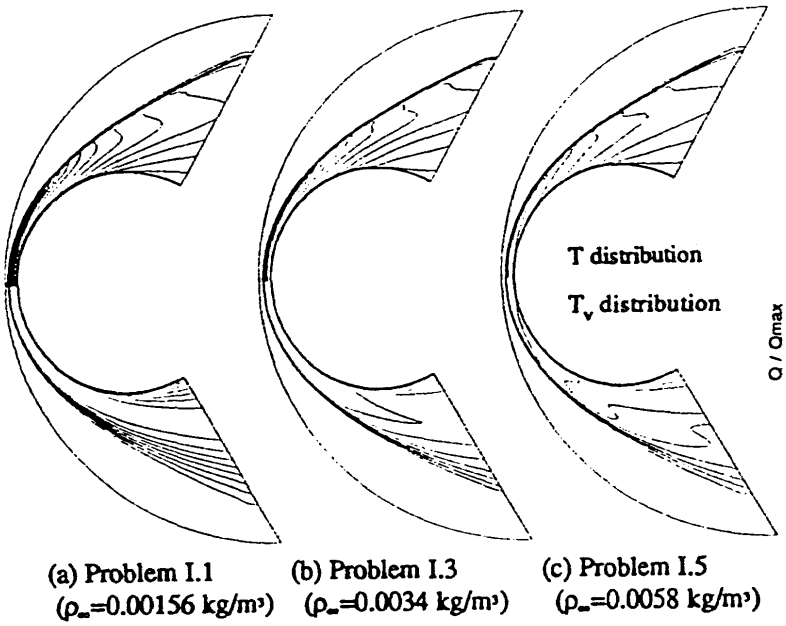

Fig. 5 Temperature distribution for Problem I

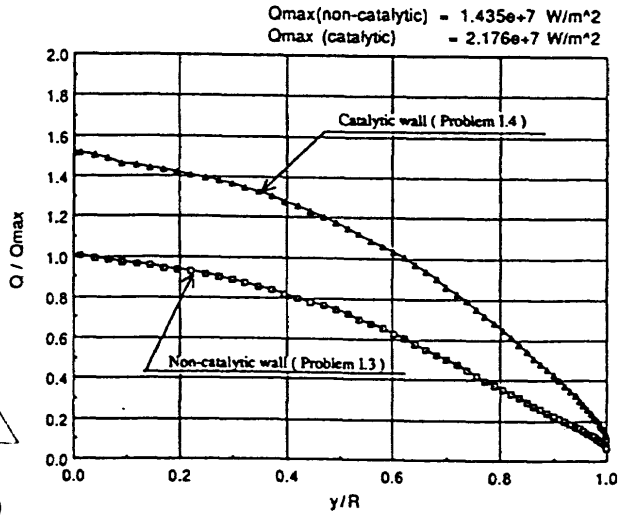

Fig. 7 Heat flux distribution for Problem I.3 and 4

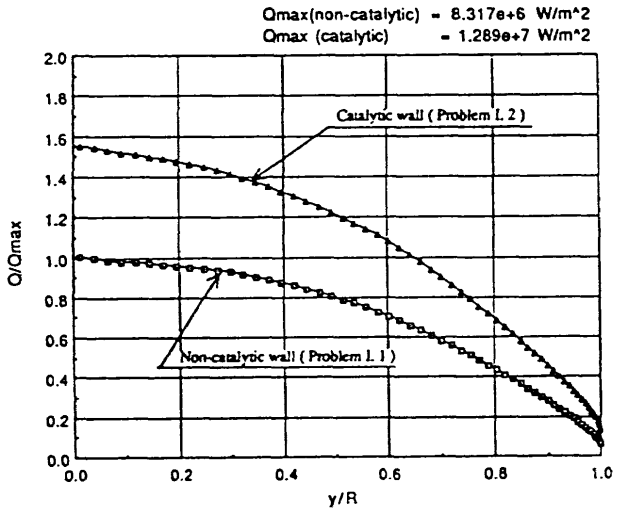

Fig. 6 Heat flux distribution for Problem I.1 and 2

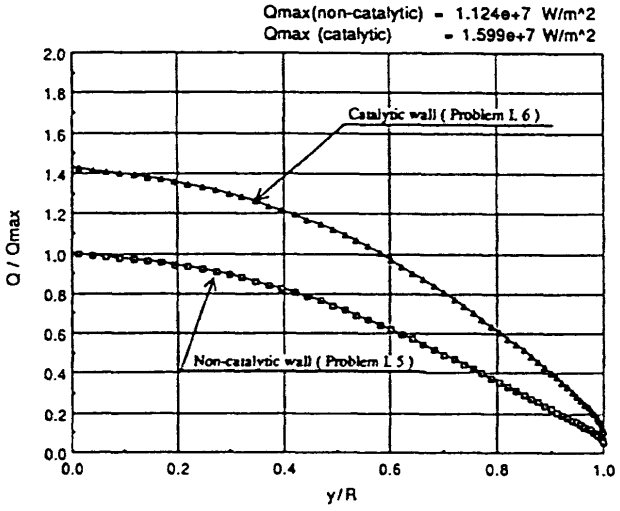

Fig. 8 Heat flux distribution for Problem I.5 and 6

Figure 11 shows the translational temperature distribution for Problem II.2. Since the altitude corresponding to the free stream conditions for this problem is lower than the one for Problem II.1 and the free stream density and pressure are relatively high, very sharp shock wave is captured. A comparison of the heat flux distribution along the wall for the non-catalytic (Problem II.2) and the catalytic (Problem II.3) case in Figure 12 shows that the stagnation heat flux of a catalytic wall case is about 1.8 times higher than that of a non-catalytic wall

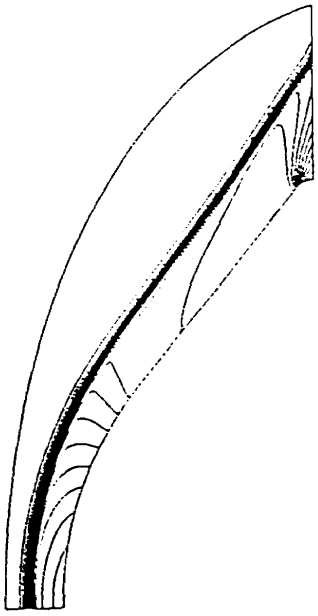

Fig. 9 Pressure distribution for Problem II.1

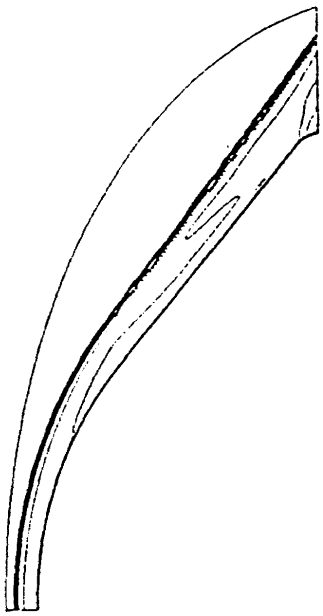

Fig. 11 Translational temperature distribution for Problem II.2 (T_{max} = 1.32 ×10^4 K)

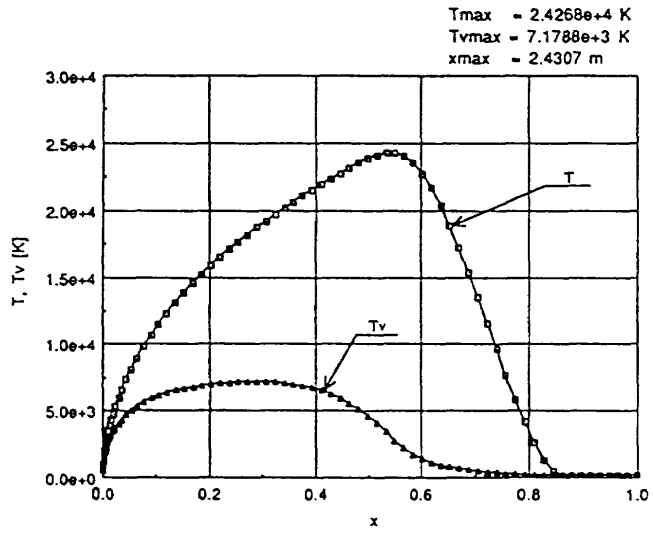

Fig.10 Translational and vibrational temperature distribution along the stagnation streamline for Problem II.1

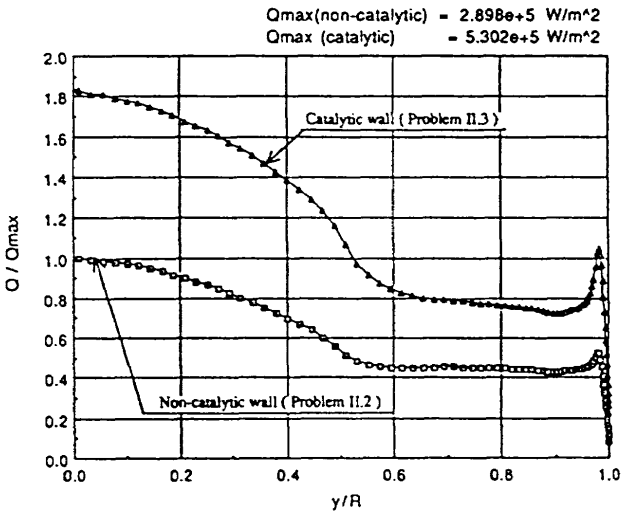

Fig. 12 Heat flux distribution for Problem II.2

case.

Problem IV is a very challenging case for a numerical analysis since both the very strong non-equilibrium shock layer around the forebody and the very complicated flow structures around the afterbody must be captured. Especially, the latter include the rapid expansion at the shoulder, the separation of the flow on the backside of the body, the shear layer and the recompression shock in the back flow region, which are now becoming to be main subjects of research in hypersonic aerodynamics.

Figure 13 and 14 are the translational and vibrational temperature distribution for Problem IV.1 respectively. They clearly show these flow characteristics mentioned above. More careful observation of the numerical results indicates that the flow in the recirculation zone becomes supersonic of about Mach 2, therefore, the shock appears at the corner just after the body.

Figure 15 and 16 show the heat flux distribution along the wall for the non-catalytic (Problem IV.1) and catalytic wall case (Problem IV.2) respectively. The small disturbance of the heat flux just after the body observed in both cases also indicates the existence of the shock in the recirculation zone. However, the increase of the heat flux after the reattachment point (where x / L is about 0.6) is not so high as expected. More careful analyses and comparison with experimental results are necessary in order to determine whether this is real physical phenomenon or caused by some numerical errors such as mesh intervals or physical models applied here.

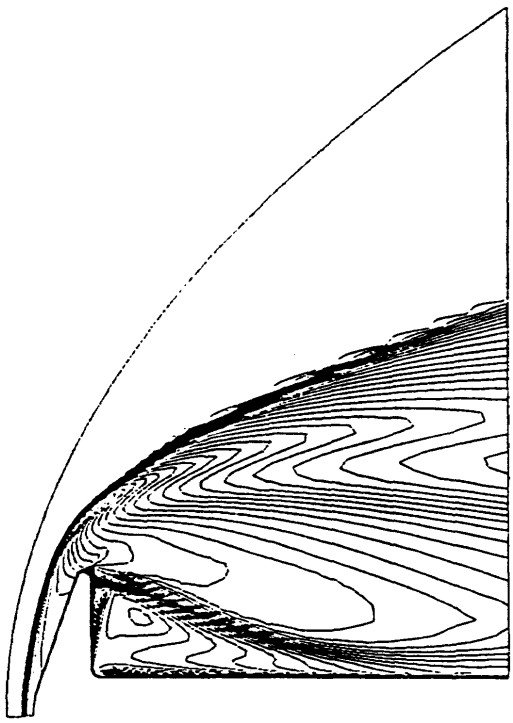

Fig.14 Vibrational temperature distribution for Problem IV.1 (T_{vmax} = 6.26 ×10^3 K)

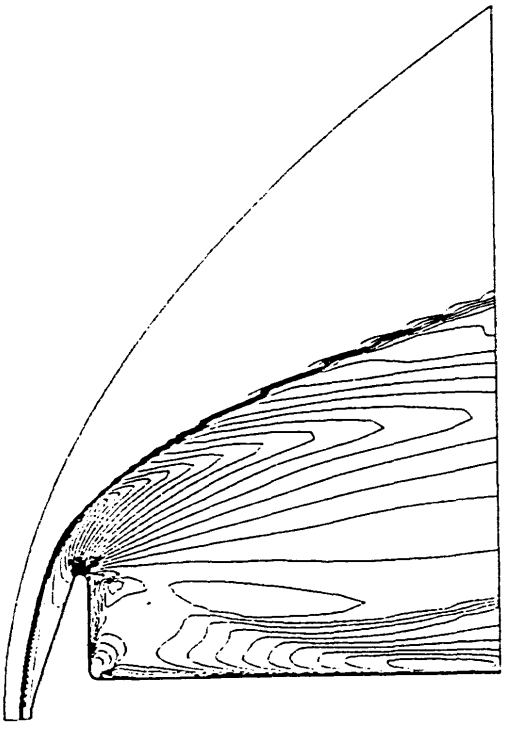

Fig. 13 Translational temperature distribution for Problem IV.1 (T_{max} = 9.20 ×10^3 K)

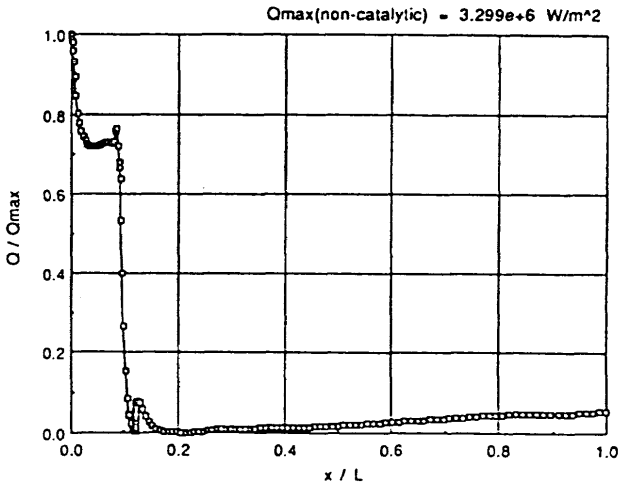

Fig 15 Heat flux distribution for Problem IV.1 (Non-catalytic wall case)

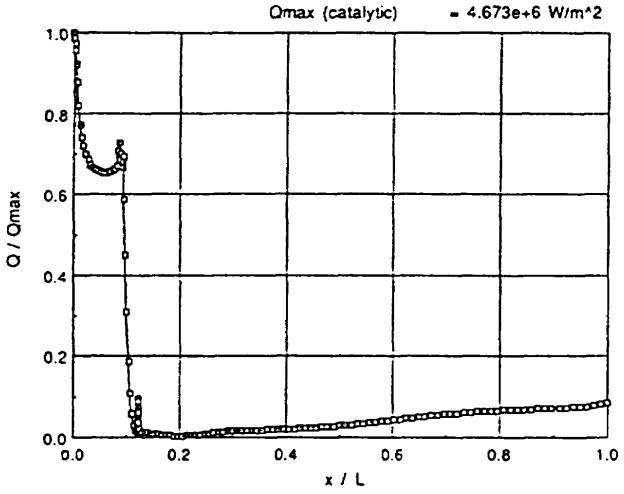

Fig 16 Heat flux distribution for Problem IV.2
(Catalytic wall case)

6. Conclusion

In this paper, brief outlines of physical assumptions and numerical methods applied to calculate several non-equilibrium hypersonic flows are mentioned and some numerical results of them are presented and discussed.

Axisymmetric full Navier-Stokes equations which have chemically and thermally nonequilibrium effects are considered by using Park's two-temperature model and the vibrational relaxation model from the SSH theory. For the time integration, an efficient numerical algorithm of an implicit finite difference method is used, which consists of the combination of LU-SGS scheme and the implicit diagonal method for a source Jacobian matrix. For convective terms, AUSMDV scheme generalized into the nonequilibrium flow case is applied.

Several types of flow cases are investigated; Problem I (Sphere cases), Problem II.1-3 (Orex cases) and Problem IV. 1-2 (Spherically Blunted Cone cases). All cases indicate that the flow inside the shock layer is in strong nonequilibrium and very complex real gas effects are observed. The comparison of heat fluxes between the catalytic and non-catalytic walls shows that the stagnation heat flux for catalytic wall cases are about 1.5-1.8 times higher than those for non-catalytic cases.

It is shown that fairly reasonable results can be obtained with both numerical methods and physical models applied here. However, numerical results of some cases indicate that more careful analyses and comparison with experimental results are necessary in order to clarify the more complex flow structures in the back flow region, for example, of Problem IV in this study.

References

[1] Park,C., Nonequilibrium Hypersonic Aerothermodynamics, John Wiley & Sons, Inc., 1990.

[2] Gnoffo, P.A., Gupta, R.N. and Shinn , J.L., "Conservation Equations and Physical Models for Hypersonic Air Flows in Thermal and Chemical Nonequilibrium", NASA TP-2867, 1989.

[3] Yoon,S. and Kwak,D., "Implicit Methods for the Navier-Stokes Equations", Computational Technology for Flight Vehicles, Vol. I, pp.535-547, 1990.

[4] Eberhardt, S. and Imaly, S., "A Diagonal Implicit Scheme for Computing Flows with Finite-Rate Chemistry", AIAA Paper 90-1577, 1990.

[5] Kurotaki, T., "Numerical Analysis of Two Dimensional / Axisymmetric Non-equilibrium Hypersonic Flow", NAL SP-19, pp.93-98, 1992.

[6] Wada, Y. and Liou, M.-S., "A Flux Splitting Scheme with High-Resolution and Robustness for Discontinuities", AIAA Paper 94-0083, 1994.

[7] Schwartz, R.N., Slawsky, Z.I. and Herzfeld, R.N., "Calculation of Vibrational Relaxation Times in Gases", J. Chem. Phys., 20, PP. 1591-1599, 1954 .

[8] Thivet, F., Perrin, M.Y. and Candel, S., "A Unified Nonequilibrium Model for Hypersonic Flows", Phys. Fluids, A3, pp. 2799-2812, 1991.